Learning Non-Euclidean Representations With SPD Manifold for Myoelectric Pattern Recognition

Dezhen Xiong, Daohui Zhang, *Member, IEEE*, Xingang Zhao, *Member, IEEE*, Yaqi Chu, and Yiwen Zhao

***Abstract*— How to learn informative representations from Electromyography (EMG) signals is of vital importance for myoelectric control systems. Traditionally, hand-crafted features are extracted from individual EMG channels and combined together for pattern recognition. The spatial topological information between different channels can also be informative, which is seldom considered. This paper presents a radically novel approach to extract spatial structural information within diverse EMG channels based on the symmetric positive definite (SPD) manifold. The object is to learn non-Euclidean representations inside EMG signals for myoelectric pattern recognition. The performance is compared with two classical feature sets using accuracy and F1-score. The algorithm is tested on eleven gestures collected from ten subjects, and the best accuracy reaches 84.85%±5.15% with an improvement of 4.04%∼20.25%, which outperforms the contrast method, and reaches a significant improvement with the Wilcoxon signed-rank test. Eleven gestures from three public databases involving *Ninapro DB2, DB4, and DB5* are also evaluated, and better performance is observed. Furthermore, the computational cost is less than the contrast method, making it more suitable for low-cost systems. It shows the effectiveness of the presented approach and contributes a new way for myoelectric pattern recognition.**

***Index Terms*— EMG, non-Euclidean, SPD manifold, Log-Euclidean metric, pattern recognition.**

Manuscript received December 6, 2021; revised April 26, 2022; accepted May 18, 2022. Date of publication May 27, 2022; date of current version June 10, 2022. This work was supported in part by the National Natural Science Foundation of China under Grant U1813214, Grant U20A20197, Grant 61773369, Grant 61903360, and Grant 92048302; in part by the Self-Planned Project of the State Key Laboratory of Robotics under Grant 2020-Z12; in part by the Liaoning Revitalization Talents Program under Grant XLYC1908030; and in part by the China Postdoctoral Science Foundation Funded Project under Grant 2019M661155. *(Corresponding authors: Xingang Zhao; Daohui Zhang.)*

This work involved human subjects or animals in its research. Approval of all ethical and experimental procedures and protocols was granted by the Ethical Committee of the Shenyang Institute of Automa tion, Chinese Academy of Sciences.

Dezhen Xiong is with the State Key Laboratory of Robotics, Shenyang Institute of Automation, Chinese Academy of Sciences, Shenyang 110016, China, also with the Institutes for Robotics and Intelligent Manufacturing, Chinese Academy of Sciences, Shenyang 110169, China, and also with the University of Chinese Academy of Sciences, Beijing 100049, China (e-mail: xiongdezhen@sia.cn).

Daohui Zhang, Xingang Zhao, Yaqi Chu, and Yiwen Zhao are with the State Key Laboratory of Robotics, Shenyang Institute of Automation, Chinese Academy of Sciences, Shenyang 110016, China, and also with the Institutes for Robotics and Intelligent Manufacturing, Chinese Academy of Sciences, Shenyang 110169, China (e-mail: zhangdaohui@sia.cn; zhaoxingang@sia.cn; chuyaqi@sia.cn; zhaoyw@sia.cn).

Digital Object Identifier 10.1109/TNSRE.2022.3178384

I. Introduction

ELECTROMYOGRAPHY (EMG) signal is the faint physiological signal which can be accessed during muscle contraction. EMG signal is composed of motor unit action potentials (MUAPs) generated by muscle fibers. It can be classified into surface EMG and invasive EMG [1]. The former is collected by electrodes above the skin, whilst the latter is by needle electrodes inserted in muscles. Other sensors for human movement analysis, like inertial measurement unit (IMU) [2], camera [3], data glove [4], etc., reflect human intentions at the physical level, which means they work only if the human body really moves. Those sensors are effective for healthy subjects but not for abnormal subjects who have motor nerve diseases or limb loss. EMG signals contain physiological level information from which the movement intention of abnormal subjects can be decoded. It has excellent potential for human-machine interaction tasks like prosthesis control [5], stroke rehabilitation [6], etc., which is more intuitive than the physical level method.

How to decode human movement intentions from EMG signals accurately is crucial for an EMG-based human-machine interface (HMI). One approach usually used for EMG-based HMI is the model-based method, which employs the kinematic model or the musculoskeletal model for movement estimation [7]. It is suited for low degree-of-freedom (DOF) tasks like movements of the elbow, ankle, etc., which is not appropriate for multi-DOF tasks like hand gesture classification. Another popular approach is the model-free method [7], which uses machine learning algorithms for pattern recognition. It consists of several processes, containing signal preprocessing, feature extraction, and pattern recognition, among which feature extraction occupies an important position.

There has been plenty of research exploiting statistical features such as time-domain features, frequency-domain features, and time-frequency domain features [8], which leads to

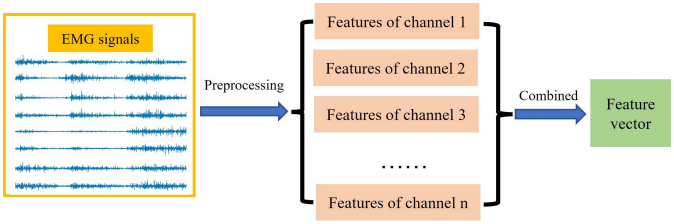

Fig. 1. Diagram illustration of classical feature extraction approach. The EMG signals are preprocessed at first. Then features of every channel are extracted and combined to construct feature vectors for pattern recognition.

the prosperity of EMG feature engineering. Those features are usually calculated from each channel separately and concatenated as a vector, as shown in Fig. 1, leaving structural features among different channels seldom considered. EMG signal is unstable temporally, but constant information may exist within channels spatially. Exploiting latent topological structures is a geometric approach, which can be a novel perspective for accurate and efficient EMG decoding.

There have been some studies on this issue. For high-density (HD) EMG signals, a handful of research has focused on spatial features in recent years. Jordanic *et al.* [9] predict four actions under three force levels of spinal cord injury (SCI) patients using hybrid spatial information of HD-EMG signals, which significantly outperforms the other two feature sets. Xie *et al.* [10] propose a multiscale two-directional two-dimensional principal component analysis (MS2D^{2}PCA) approach to extract spatial information above time-frequency representations of HD-EMG data, and performance above 96% is observed on twenty gestures of twelve stroke survivors. For sparse channel EMG signals, muscle synergy can be viewed as a spatial feature because it simultaneously extracts information from multiple channels [11]. It represents high-level neural control information of the Central Nervous System (CNS) on muscle groups [12]. It usually needs to attach electrodes on specific muscles, and it's more suitable for motion mechanism-related research as neural drives. More informative spatial features of sparse channel EMG signals are worth being explored.

The classical feature extraction method operates EMG signals in a flattened Euclidean geometric space with statistical features, which may not be enough to express the underlining information inside it. Riemann manifold belongs to non-Euclidean geometry, which studies geometric properties on the nonlinear curved space. It can be divided into several categories: Grassmann manifold, Stiefel manifold, symmetric positive definite (SPD) manifold, *etc.* [13] SPD manifold is a cone manifold defined by the Riemannian metric [14], which chooses SPD matrices like covariance matrix as the input. It is convenient for calculating, which makes it popular for learning representations from data.

SPD manifold has been widely used in computer vision [15], machine learning [16], medical imaging [17], brain-computer interfaces [18], etc. Tuzel *et al.* [15] detect pedestrians from the image using covariance descriptor for feature representation and LogitBoost for classification. Gao *et al.* [16] present a new distance measure on SPD manifold for similarity-based classification, which shows superior performance on visual classification tasks. Das *et al.* [17] propose a sparse coding and dictionary learning scheme on SPD manifold for breast cancer evaluation. Tang *et al.* [18] present a generalized learning Riemannian space quantization (GLRSQ) algorithm with SPD matrices as the input. In general, the SPD manifold has more discriminative metrics than Euclidean geometry for feature extraction [19], which makes it successful on various types of data. SPD manifold has the advantage of simplicity, flexibility, and effectivity [20], which makes it a good alternative for learning representations from physiological signals. Nevertheless, it remains unexplored for EMG-based hand gesture classification tasks as far as we have known.

This work extracts intrinsic structural information inside EMG envelopes for myoelectric recognition employing the SPD manifold. The proposed SPD manifold-based myoelectric pattern recognition framework is depicted in Fig. 2. Raw EMG data is firstly preprocessed and converted into SPD matrices. Then, the geometric mean of the training set SPD matrices is calculated, and the SPD matrices are projected toward a tangent space at their geometric mean. After that, a tangent feature matrix is flattened and dimension reduced for pattern recognition. The main novelty of this research can be two folds: On one hand, this is the first time that an SPD manifold is used to extract spatial non-Euclidean structural representations from EMG signals for hand gesture classification as far as we can know. On the other hand, the presented approach significantly shrinks the computational consumption while reaching remarkable performance. Our contribution to this work can be summarized as follows:

1) A framework for EMG-based gesture classification is established using non-Euclidean representation extracted by the SPD manifold-based method.
2) The superiority of the SPD manifold-based scheme is verified by comparing it with several classical feature sets for hand gesture classification.
3) The effectiveness of the proposed approach is verified on hand gestures of self-collected data and public data with various EMG sensors and data formats.
4) The classification performance, computation time, and significance superiority are introduced to analyze the SPD manifold-based approach comprehensively.

The remainder of this paper is arranged as follows: Basic knowledge of principles and attributes for SPD manifold is described in section II. The proposed method, contrast method, experiment data, evaluation standards, etc., are illustrated in section III. In section IV, the result is presented. Section V makes discussions about this work. The last part is about the conclusion and prospective works.

II. SPD Manifold

In this section, some basic notions and important attributes like geometry distance, exponential/logarithm map of SPD manifold will be introduced, which are the mathematical foundations of the proposed method.

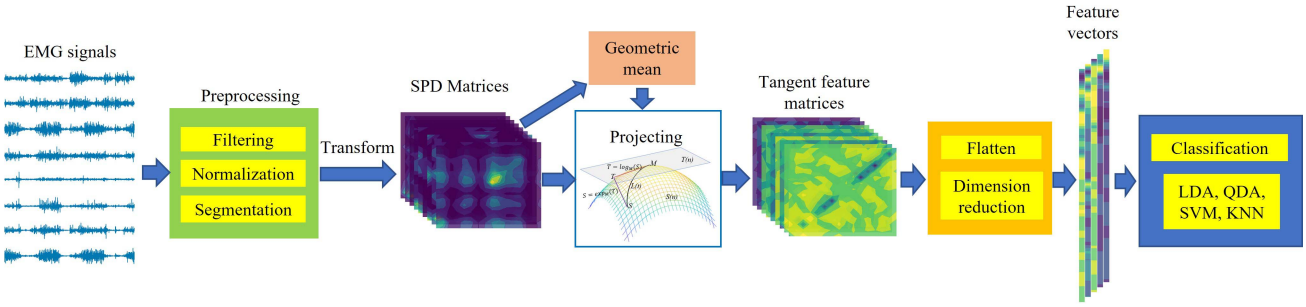

Fig. 2. The general procedure of the proposed method.

A. Notions

For a matrix S with the shape of $n*n$, if it satisfies $uSu^T > 0$ for any vector u, which is a non-zero vector, then S will be a positive definite matrix. If $S = S^T$ holds, matrix S is symmetric. An SPD matrix S can be established if the above two conditions hold at the same time.

$$S(n) = \{S \in R^{n*n} : u^T Su > 0 \wedge S = S^T \ \forall u \in R^n \wedge u \neq \vec{0}\} \tag{1}$$

where $\vec{0}$ represents for a zero vector. Since an SPD matrix with the shape of $n \times n$ satisfies symmetric, it has $n(n+1)/2$ independent parameters.

The SPD manifold has the following properties [21]:

1) $\forall S \in S(n),\ \det(S) > 0$
2) $\forall S \in S(n),\ S^{-1} \in S(n)$
3) $\forall S_1,\ S_2 \in S(n),\ S_1 S_2 \in S(n)$

B. The Exponential and Logarithmic Function of Matrix

The exponential function *expm(*)* and logarithmic function *logm(*)* of matrix S can be expanded into a *Taylor* series:

$$expm(S) = \sum_{n=0}^{\infty} \frac{S^n}{n!}$$
$$logm(S) = -\sum_{n=1}^{\infty} \frac{(I-S)^n}{n}$$

Matrix S can be decomposed into the following form by eigenvector decomposition:

$$S = Udiag(\alpha_1, \alpha_2, \ldots, \alpha_n)U^T$$

where matrix U is the eigenvector matrix of matrix S, $\alpha_1, \alpha_2, \ldots, \alpha_n$ are eigenvalues of a matrix S. Since that S is symmetric, matrix U satisfies $U^T = U^{-1}$. Therefore, the exponential and logarithmic form of matrix S can be transformed into the following format [16]:

$$expm(S) = U\text{diag}(\exp(a_1), \exp(a_2), \ldots, \exp(a_n))U^T \tag{2}$$
$$logm(S) = U\text{diag}(\log(a_1), \log(a_2), \ldots, \log(a_n))U^T \tag{3}$$

Through the above transformation of equations (2) and (3), the exponential and logarithmic operation of a matrix is more computationally efficient.

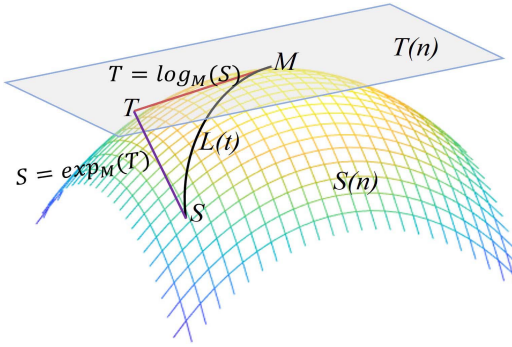

Fig. 3. Illustration of *exponential* map operator $exp_M(*)$ and *logarithmic* map operator $log_M(*)$. The $exp_M(*)$ operator transforms matrix T from the tangent space $T(n)$ to the SPD manifold at M. The $log_M(*)$ converts matrix S back towards the tangent space. $L(t)$ represents the *geodesic* between S and M.

C. The Exponential and Logarithmic Map

The tangent space plays a vital role in analyzing the SPD manifold. Given M on the manifold, the corresponding tangent space $T_M(n)$ represents for all possible tangent vectors that go through M. For an SPD matrix $S \in S(n)$, it can be projected towards the tangent space at matrix M employing the *logarithmic* operation $log_M : S \to T_M S$. The matrix T in tangent space can be viewed as the derivative of S along with M. The inverse of it, which can be called the *exponential* map, converts the matrix in tangent space to the SPD manifold, described by $exp_M : T \to S_M T$. The process is illustrated in Fig. 3.

Under the condition of different geometry metrics, the *logarithmic* map operator and the *exponential* map operator will be in different formations. The mathematical formula under specific metrics will be introduced in the following section E.

D. Geometric Mean

For a set of SPD matrices $\{S_i, i = 1, 2, \ldots, n\}$, their geometric mean, which can also be called the Riemannian mean or *Fréchet* mean [22] is defined as the minimum summation of squared distances for all the SPD matrices, as illustrated by the following equations [22]:

$$M = arg\,min_M \sum_{i=1}^{n} \delta^2(M, S_i) \tag{4}$$

where $\delta(*)$ represents the geometric distance of two SPD matrices.

Employing the Euclidean metric, the mean value for a series of SPD matrices satisfies the smallest summation of squared Euclidean distance toward other SPD matrices according to (4). It can be named the *arithmetic* mean, which can be calculated by averaging them, as illustrated by [22]:

$$M(S_1, S_2, \cdots, S_n) = \frac{1}{n}\sum_{i=1}^{n} S_i \tag{5}$$

However, it is not appropriate under some circumstances due to factors like the *swelling effect* [23]. More suitable metrics, which will be introduced in the following parts, are desired to describe the SPD manifold's geometry attributes.

E. Geometry Metric

The notion of metric represents an operator that measures the distance of two elements. In the Euclidean space, the Euclidean metrics have been widely used. The shortest distance between two points is a straight line in Euclidean space. However, the Euclidean metric is not suitable for curved space like the SPD manifold space, in which the shortest distance for two points on the SPD manifold is a curved line called *geodesic*. Metrics like Affine-Invariant Metric (*AIM*) [24], Log-Euclidean Metric (*LEM*) [23], and Bregman divergences like Stein divergence [25] can be used to measure the geometry distance of it. Under different metrics, the ways to calculate geometry distance, exponential and logarithmic maps, and geometry means will be in various formats.

The geometry of the SPD manifold can be derived using *AIM*, by which the distance of X and Y is described by the following formula [14]:

$$\delta_{AIM}(X, Y) = \left\| logm(X^{-1/2} Y X^{-1/2}) \right\|_F \tag{6}$$

where $\|*\|_F$ represents the Frobenius norm. Further, the geometric mean of a series of matrices $S_i, i = 1, \cdots, n$ under this metric is given by:

$$M_{t+1} = M_t^{1/2} expm(\frac{1}{n}\sum_{i=1}^{n} logm(M_t^{-1/2} S_i M_t^{-1/2})) M_t^{1/2} \tag{7}$$

where M_t, M_{t+1} is the geometric mean for a set of matrices at t step and $t+1$ step in individual.

With Stein divergence, the geometry distance and the geometry mean are calculated by formulas (8) and (9):

$$\delta_{Stein}(X, Y) = sqrt(\log det(\frac{X+Y}{2}) - \frac{1}{2}\log det(XY)) \tag{8}$$

$$M_{t+1} = [\frac{1}{m}\sum_{i=1}^{m} (\frac{X_i + M_t}{2})]^{-1} \tag{9}$$

The above two approaches are computed repeatedly to calculate the geometric mean of a series of matrices, which takes a relatively higher time cost. What's more, complicated matrix operations like inversion, product, etc., further increase the computational complexity. A more computationally efficient approach is *LEM*, which will be introduced in the following.

The Log-Euclidean Metric on SPD manifold is on account of the Lie group structure and a new scalar product [23], through which the scalar product of two matrices S_1 and S_2 on the SPD manifold is achieved by the following [23]:

$$\langle S_1, S_2 \rangle_M = \langle D_M logm(S_1), D_M logm(S_2) \rangle \tag{10}$$

where $D_M logm(S)$ represents the directional derivative of the matrix logarithm operation for matrix S at M.

With *LEM*, the logarithmic map operator $log_M(*)$ projects matrix T_i in SPD manifold space towards the tangent space at M with [21]:

$$T_i = log_M(S_i) = D_{\log m(M)} expm(logm(S_i) - logm(M)) \tag{11}$$

where $D_{logm(M)} expm(*)$ is identical to $(D_M logm(*))^{-1}$ as derived by $logm \cdot expm = I$.

The inverse transform of it is the *exponential* map operator $exp_M(*)$ transforms matrix S_i from the tangent space back towards SPD manifold at M by the following formula [23]:

$$S_i = exp_M(T_i) = expm(logm(M) + D_M logm(T_i)) \tag{12}$$

Using the *LEM* method, the geometry distance can be achieved by equation (5) [23]:

$$\delta_{LEM}(X, Y) = \|logm(Y) - logm(X)\|_F \tag{13}$$

It only takes Euclidean computations in matrix logarithmic, which is more time-efficient than the *AIM* or Stein method.

With *LEM*, the *Fréche* mean for a set of matrices $S_i, i = 1, \cdots, n$ is given by the following formula [23]:

$$M = expm(\frac{1}{n}\sum_{i=1}^{n} logm(X_i)) \tag{14}$$

In contrast with *AIM* and Stein divergence method, *LEM* takes less computational cost, which only needs matrix logarithm and matrix exponent without matrix product, inversion, etc., and most importantly, without iteration. This paper chooses *LEM* to extract spatial information from EMG signals.

III. Methodology

A. Database

Four databases, including one self-collected and three public databases, are used in this work. The first EMG database is self-collected by ten healthy subjects (All male, Age: 24.80±0.87 years old, Weight: 68.70±7.43kg, Height: 176.90±4.87cm, Left arm: 3, Right arm: 7) without pretraining to provide natural hand gestures. The experiment involves several steps. Firstly, the skin of a participant is wiped with alcohol before the experiment. Then, a participant will sit on a chair in front of the EMG acquisition system controlled by Raspberry Pi 3B. After that, an armband named gForcePro+[1] is worn on the forearm to collect EMG data with a frequency of 400Hz. Lastly, a participant will perform hand gestures under the guidance of corresponding gestures shown on the screen, and EMG data will be collected simultaneously. The experimental scene is shown in Fig. 4(a).

[1] http://www.oymotion.com/product17/82

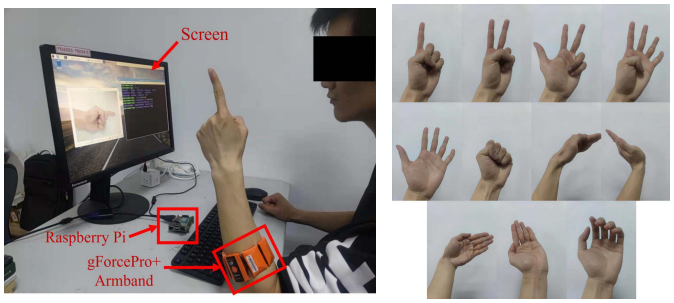

(a) (b)

Fig. 4. (a) The experimental scene of data acquisition. (b) The eleven hand gestures in this work. It contains six gestures of fingers, four gestures of the wrist, and relaxation.

There are 11 hand gestures used in this work, as shown in Fig. 4 (b). Each hand gesture lasts for 6 seconds, then follows a relaxing time of 4 seconds. Since a man needs time to react to the guidance picture, the first second of EMG data is dropped. Every gesture is repeated for six repetitions. The experiment abides by the declaration of Helsinki, and all the subjects have signed the informed consent of the experiment. We named the database '*OYData*' in the following parts to keep it simplified.

Furthermore, we use several public databases to test the proposed algorithm, including three sparse channel databases named *Ninapro* DB2, DB4, and DB5 [26]–[28]. The *Ninapro* DB2 contains 49 gestures captured from forty subjects. It is acquired with twelve wireless double–differential Delsys Trigno electrodes. There are 52 hand gestures from ten healthy participants of DB4, which are captured with twelve wireless Cometa single-differential electrodes. *Ninapro* DB5 has the same hand gesture as DB4. The EMG data is acquired with two Thalmic Myo armbands. It has a sampling frequency of 2000Hz for DB2 and DB4. For DB5, that is 200Hz. As shown in Fig. 4 (b), we select eleven gestures to test the performance. The data amount at relaxing keeps the same with other actions. All three databases have six repetitions of every movement. Four repetitions, including 1, 3, 4, 6, are used for model training, and the rest of repetitions 2, 5 are for performance evaluation on every database, respectively.

B. EMG Preprocessing

The raw data is filtered at first to remove uncorrelated noises and to keep useful information inside the raw EMG signals as much as possible. For the acquired EMG signals sampled at 400Hz, the raw data is filtered by a four-order Butterworth bandpass filter with a bound range of 10∼180Hz. And then notch filtered at 50Hz to remove powerline interference. For *Ninapro* DB2 and DB4, sampled at 2000Hz, the original data is first filtered by a four-order bandpass Butterworth filter at 10∼500Hz. Then, powerline interference is removed by a notch filter at 50Hz. For *Ninapro* DB5, sampled at 200Hz, the raw data is filtered using a four-order Butterworth bandpass filter at 10∼90Hz, and then notch filtered at 50Hz. After that, the filtered data is rectified and normalized within the range of [0, 1] employing the Min-Max normalization technique, which is defined by equation (15):

$$\overline{x} = \frac{x - min(x)}{max(x) - min(x)} \tag{15}$$

where $min(*)$ returns the minimum number of vector x, $max\ (*)$ outputs the maximum number of it.

Finally, the EMG signals are segmented into small envelopes using a sliding window with a length of 200ms and a sliding step of 50ms.

C. Learning Representations With SPD Manifold

The proposed method can be divided into two stages. Firstly, the tangent space features will be extracted. Then PCA will be used to shrink the dimension of the feature vector.

1) Feature Extraction With Tangent Space Method: The SPD manifold is utilized to learn spatial representations from EMG signals. The preprocessed data is transformed onto SPD manifold space, and the feature representations are learned. The detailed process is as follows:

Firstly, we construct an SPD matrix using EMG envelopes as the input. Research for EEG signal processing, like [21][22], chooses the covariance matrix as the SPD matrix, which needs to keep the input data with zero means. This work provides a new construction method as shown in (16):

$$S = E^T * E + I * \varepsilon \tag{16}$$

where matrix E is EMG envelope preprocessed using the procedure in *section III B*. It is with shape t^*n, where t, n are the sample length and channel number, respectively. It can be viewed as a channel-wise self-correlation matrix, which reflects the spatial structural information within different channels in that EMG data in different channels is multiplied mutually. To keep it symmetric and positive definite, a regularization term $I * \varepsilon$ is added to the matrix S, where I represents an n-dimensional identity matrix, and ε represents a small number ($\varepsilon = 1.0 * 10^{-9}$). Employing equation (16), An SPD matrix S is constructed, which contains $(n+1)\,n/2$ independent parameters.

After that, the geometry mean of all samples in the training database is calculated using the *LEM* method through equation (14). The training SPD matrices and the testing SPD matrices are transformed into the tangent space feature matrices with the following formulas:

$$F = \mathrm{logm}(S_i) - \mathrm{logm}(M) \tag{17}$$

where matrix M stands for the geometry mean of SPD matrices in the training set. A squared matrix F is flattened into a vector by the $flatten\,(*)$ operation in the following form:

$$\begin{aligned} f &= flatten(F) \\ &= [F_{11}, \ldots, F_{1n}; F_{21}, \ldots, F_{2n}; F_{n1}, \ldots, F_{nn}] \end{aligned} \tag{18}$$

Since the matrix F is symmetric, there are studies like [29] that use the $upper\,(*)$ operator to take the upper triangular of the feature matrix to get a minimum representation of it. Although the Euclidean norm of it equals geometry distances, the operation only reduces fewer than 50% of parameters and

may lose valuable information. Therefore, a more effective dimension reduction method, the principal component analysis (PCA) algorithm, is chosen in our research to produce more compact feature sets. The basic principle of PCA is described in the following part.

2) Dimension Reduction With PCA: PCA is usually used to reduce data dimension while keeping the original information reserved as much as possible. It is a linear approach that can reach remarkable performance with less computational cost. The original data is transformed toward a low-dimensional space under the consumption that the variance is maximal after transformation [30]. It aims to find an orthogonal matrix W (*shape:* n^*t), by which the original data P (*shape:* n^*m) can be transformed into low dimensional matrix Q (*shape:* t^*m), as shown in (19):

$$Q = W^T P \tag{19}$$

Every element of the matrix Q is calculated by the following formula:

$$q_{ij} = w_i p_j \tag{20}$$

In order to obtain the matrix W, the maximum variance is used as the optimization target:

$$\begin{aligned} J &= \max \left[\frac{1}{n} \sum_{i=1}^{t} \sum_{j=1}^{n} \left(w_i^T p_j - w_i^T \overline{p} \right)^2 \right] \\ &= \max \left[\sum_{i=1}^{t} w_i^T C w_i \right] \\ &\quad s.t.\ w_i^T w_i = 1 \end{aligned} \tag{21}$$

where matrix C represents the covariance matrix of matrix P, $\bar{p}$ represents the mean value of vectors p_j. The maximal loss function can be obtained while w_i, $j = 1, \ldots, t$ belong to the eigenvector of *top-t* largest eigenvalues of matrix S. The eigenvalues and eigenvectors can be obtained by algorithms like singular value decomposition (SVD). Finally, equation (19) can be solved.

3) Overall Procedure: The general process of the SPD manifold-based approach is summarized in ***Algorithm* 1**.

Algorithm 1 The Proposed Method

Input: EMG signals after preprocessing: Training set EMG_{train}, testing set EMG_{test}.

Output: Features of training and testing set: $feat_{train}$ and $feat_{test}$.

Begin

1. Constructing SPD matrix with (16) to get S_{train} and S_{test}.
2. Calculating the geometric mean M using SPD matrices S_{train} with formula (14).
3. Projecting SPD matrices onto tangent feature space with formula (17).
4. Flattening feature matrices into feature vectors with formula (18).
5. Dimension reduction using PCA to get $feat_{train}$ and $feat_{test}$. The reduced dimension is $2n$, where n is the channel number.

End

Return $feat_{train}$, $feat_{test}$

D. Pattern Classification

Once spatial representations $feat_{train}$ and $feat_{test}$ are extracted from EMG data, then machine learning algorithms are employed for pattern recognition. A model will be trained using data from the training set, and its performance will be evaluated using data from the testing set. Four supervised pattern recognition algorithms that are usually used in related hand gesture recognition tasks with EMG signals [27], [31] involving Linear Discriminant Analysis (LDA), Quadratic Discriminant Analysis (QDA), K-Nearest Neighbors (KNN), and Support Vector Machine (SVM) are employed for hand gesture classification. These machine learning algorithms are implemented by a python toolbox named *scikit-learn* with the version of 0.24.2 [32].

E. Baseline Methods

To show the effectiveness of the presented feature extraction method, we compared it with classical feature sets involving: the time-domain (TD) feature set [26], [33], the marginal discrete wavelet transform (mDWT) [26], [34] feature set, TD-spatial (TDs), mDWT-spatial (mDWTs), and muscle synergy.

The TD method is a feature set that combines four classical features, involving mean absolute value (MAV), slope-sign change (SSC), waveform length (WL), and zero-crossing (ZC). The mDWT method extracts time-frequency domain features using discrete wavelet transform. This work chooses a three-level 'db7' mother templet for feature extraction, keeping the same with [26]. The spatial features are also extracted by TD and mDWT. A spatial matrix in equation (16) is used as the input to construct TDs and mDWTs.

The EMG signals are preprocessed using the same steps as the SPD manifold-based method. The feature vector of TD, TDs, mDWT, and mDWTs is normalized by the z-score normalization method, as described in equation (22), to keep the component of the feature vector in the same range and to improve the classification performance.

$$x_{norm} = \frac{x - mean(x)}{std(x)} \tag{22}$$

where $mean(*)$ returns the mean value of x, $std(*)$ gives the standard deviation.

Besides, synergy features are extracted with non-negative matrix factorization (NMF) at two dimensions (Refer to [12]) for spatial feature extraction. After feature extraction, machine learning algorithms are used for pattern recognition. The parameters of the classifier are in accordance with the SPD manifold-based method to make a fair comparison. The overall processing scheme of the proposed method and the contrast group is shown in Fig. 5.

F. Performance Evaluation Standards

The performance of algorithms in this work is evaluated by classification accuracy and F1-score. Accuracy is the most

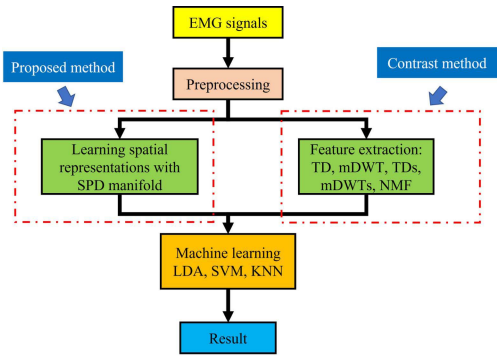

Fig. 5. The general processing scheme of relevant algorithms in this work.

common standard usually used in classification tasks. The formula of it is defined by equation (23):

$$\text{Accuracy} = \frac{\text{Correctedly predicted samples}}{\text{All samples}} * 100\% \quad (23)$$

Since the EMG signals of the *Ninapro* database have been relabeled, the data amount of classes for each gesture may not be equal to each other. The F1-score is suited for conditions where the categories of samples are unbalanced, which can be calculated as the harmonic mean of precision and recall, as described in equation (24):

$$F1\ score = 2 * \frac{Precision * Recall}{Precision + Recall} \quad (24)$$

in which *Precision* and *Recall* are determined by the following formula:

$$Precision = \frac{TP}{TP + FP}$$
$$Recall = \frac{TP}{TP + FN}$$

where operator *TP*, *FP*, and *FN* standards for true positive, false positive, and false negative in respective. The result for every label is weighted by the samples number of every class to calculate the F1-score.

The Wilcoxon signed-rank test [35] is used to analyze whether a significant difference exists between the proposed method and the contrast method employing a significance level of 0.05 ($p<0.05$) by default. There is a considerable difference between the input samples if p <0.05 holds, and one approach will be significantly better than the other.

IV. Result

This section will present classification accuracy and F1-score on four databases. The Wilcoxon signed-rank test will be made for significance analysis of the SPD manifold-based method compared with two classical methods. The default format of classification accuracy and F1-score is mean±standard deviation.

A. Performance on OYData

The classification accuracy on the presented database is shown in Table I. The best accuracy is 84.85%±5.15%, which is achieved by the proposed SPD manifold-based approach with an SVM classifier, and an improvement of 4.04%∼20.25% is achieved against contrast methods. The SVM classifier is nonlinear with a radial basis function (RBF) kernel. Employing LDA, the progress of about 5.52%∼15.25% can be observed. By QDA, the progress reaches 2.76%∼33.98%. For KNN, the improvement is 3.96%∼15.02%. It shows that our approach outperforms contrast methods based on all classifiers on this database.

TABLE I
Classification Performance (%) on *OYDATA*

Method	LDA	QDA	KNN	SVM
TD	73.37±6.54	46.61±3.54	67.61±6.10	80.01±5.94
TDs	64.89±8.36	73.56±6.74	67.38±4.79	64.60±8.07
mDWT	73.97±6.01	77.83±5.66	78.48±5.83	80.81±5.42
mDWTs	66.97±6.93	75.92±7.76	77.61±4.82	**77.02**±8.11
NMF	74.62±7.38	77.46±5.40	76.19±6.02	79.42±6.19
SPD	80.14±5.03	80.59±4.60	82.44±5.47	**84.85±5.15**

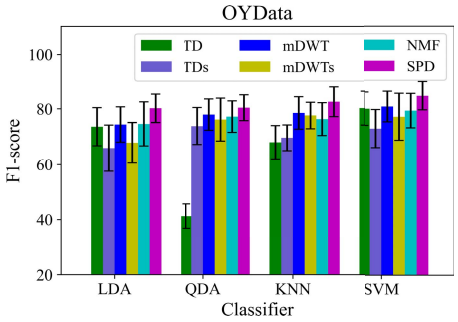

Fig. 6. The F1-score of the proposed method and the contrast method on the presented database.

The F1-score is used to describe the performance under the condition that the samples of every label are unbalanced. The performance utilizing the F1-score is shown in Fig. 6. The best F1-score is 84.95%±5.09%, achieved by the proposed method with an SVM classifier. It offers a similar trend with classification accuracy in general. The confusion matrix of the presented approach with an SVM classifier is depicted in Fig. 7, through which good performance is observed.

B. Performance on Ninapro

The classification accuracy on the same 11 gestures of Ninapro DB2, DB4, and DB5 is shown in Table II. For *Ninapro* DB2, which contains data from 40 subjects, the best accuracy reaches 81.93%±5.96% using the proposed method and SVM classifier, and the increment of 2.02%∼25.24% is reached compared with the contrast group. Employing LDA, comparable performance is achieved with TD, and an improvement of about 5.01%∼13.23% can be observed against others. By QDA, the progress reaches 5.56%∼21.62%. With KNN, the improvement is 4.60%∼16.36%.

For *Ninapro* DB4, which includes EMG data from 10 healthy subjects, the best performance is 81.75%±7.28%, achieved by SVM with the presented method. With the SVM

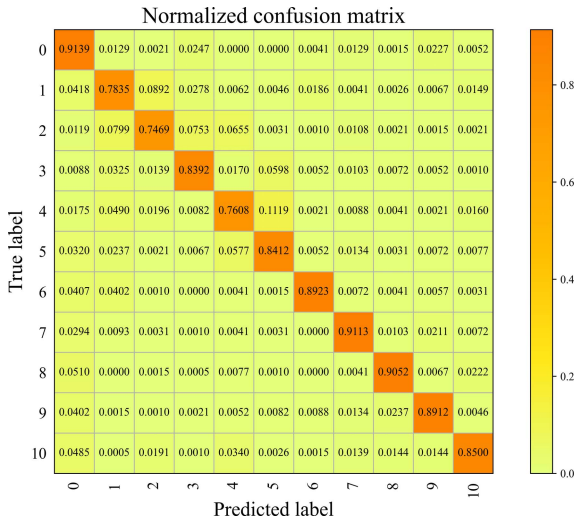

Fig. 7. The normalized confusion matrix of the SPD manifold-based method using an SVM classifier.

TABLE II
CLASSIFICATION ACCURACY (%) ON 11 GESTURES OF *NINAPRO* DB2, DB4, AND DB5

DB	Method	LDA	QDA	KNN	SVM
DB2	TD	73.67±6.91	56.33±9.19	73.13±7.67	79.91±6.19
	TDs	61.21±7.88	61.22±9.88	61.84±7.25	66.69±8.34
	mDWT	68.40±6.58	72.39±8.84	73.60±8.14	77.89±6.79
	mDWTs	60.18±6.92	65.55±9.72	70.72±7.52	66.96±8.20
	NMF	65.18±8.12	57.43±27.07	65.89±7.52	71.37±7.57
	SPD	73.41±7.52	77.95±6.59	78.20±6.33	**81.93±5.96**
DB4	TD	73.78±9.00	54.34±9.91	74.46±8.91	79.79±7.44
	TDs	57.96±10.37	63.45±10.20	58.44±7.87	63.21±9.91
	mDWT	65.93±8.91	72.88±9.06	74.03±9.85	77.35±9.47
	mDWTs	56.10±8.39	65.87±10.16	70.88±8.76	64.11±9.58
	NMF	64.79±10.53	60.13±27.68	68.45±7.80	71.75±8.75
	SPD	73.44±9.49	78.72±7.44	78.67±8.05	**81.75±7.28**
DB5	TD	70.02±4.33	47.33±9.27	62.66±5.86	75.11±4.16
	TDs	65.96±4.71	63.67±5.19	62.85±7.07	70.52±60.18
	mDWT	68.88±4.77	69.45±5.57	76.03±4.55	78.48±4.19
	mDWTs	65.36±6.21	67.04±6.17	75.86±4.03	71.67±5.45
	NMF	72.62±3.24	76.33±3.59	66.85±5.35	76.49±3.62
	SPD	76.98±4.13	79.58±3.85	81.77±4.14	**84.52±3.63**

classifier, the performance is higher than the contrast group, with an improvement of 1.96%∼18.54%. With LDA, the proposed method is slightly lower than TD with a drop of 0.34% but higher than others with an improvement of 7.51%∼17.34%. Employing classifiers of QDA, KNN, the progress of 5.84%∼24.38%, 4.21%∼20.23% can be achieved.

For *Ninapro* DB5, which involves EMG data of 10 subjects captured by two Myo armbands, the best performance reaches 84.52%±3.63% with the presented method and SVM classifier, which gets an improvement of 6.04%∼14.00% than other methods. For the other three classifiers involving LDA, QDA, and KNN, the proposed method reaches the improvement of 4.36%∼11.62%, 3.25%∼32.25%, and 5.74%∼19.11% to contrast methods.

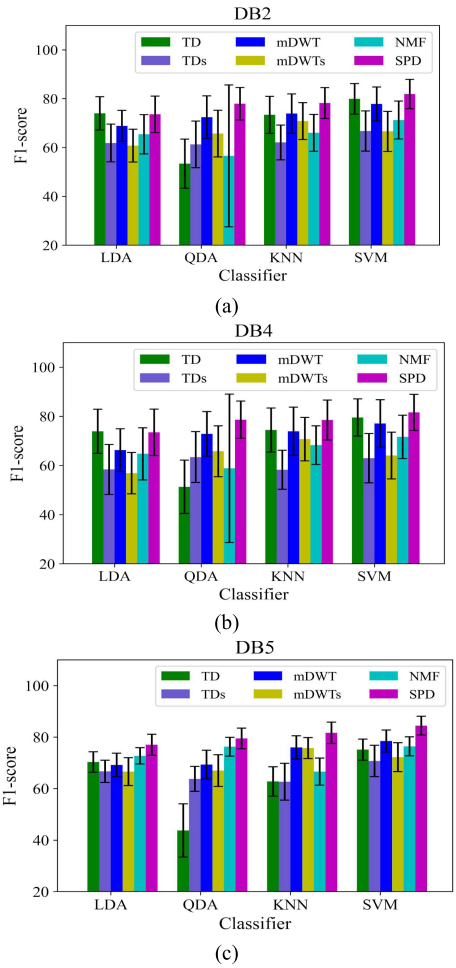

Fig. 8. Figure (a)∼(c) is in accordance with the F1-score on 11 hand gestures from *Ninapro* DB2, DB4, and DB5.

The F1-score on *Ninapro* DB2, DB4, and DB5 is shown in Fig. 8. (a)∼(c). The best F1-scores on DB2, DB4, and DB5 are 81.90%±6.00%, 81.60%±7.34%, and 84.45%±3.66% achieved by the SPD manifold-based method with an SVM classifier. It reaches a higher F1-score than other classifiers using any feature set, which shows a similar trend to classification accuracy in Table II.

C. Statistic Significance

The statistical significance of the proposed method against contrast methods using an SVM classifier on all four databases is summarized in Table III. The p-value is calculated using the classification accuracy of all the subjects between the presented approach and the contrast approach employing the Wilcoxon signed-rank test. The SPD manifold-based method is significantly better than other approaches on *OYData* and *Ninapro* DB2, DB4, and DB5, because $p < 0.05$ holds on all these databases. In general, the SPD manifold-based method is effective, outperforming the contrast method numerically and statistically.

D. Computational Cost

Compared with the contrast group, the computation consumption of the proposed SPD manifold-based method against

TABLE III
THE STATISTICAL SIGNIFICANCE LEVEL OF THE PROPOSED METHOD AGAINST THE CONTRAST METHOD USING AN SVM CLASSIFIER

Method	*OYData*	DB2	DB4	DB5
TD	p<0.005	p<0.0001	p<0.01	p<0.005
TDs	p<0.005	p<0.0001	p<0.005	p<0.005
mDWT	p<0.005	p<0.0001	p<0.005	p<0.005
mDWTs	p<0.005	p<0.0001	p<0.005	p<0.005
NMF	p<0.005	p<0.0001	p<0.005	p<0.005

TABLE IV
COMPUTATIONAL COST (MILLISECOND) OF EVERY INDIVIDUAL SAMPLE

Database	TD	TDs	mDWT	mDWTs	NMF	SPD
OYData	0.962	0.246	0.681	0.504	3.167	0.092
DB2	6.135	0.460	1.758	0.774	4.133	0.187
DB4	6.152	0.468	1.785	0.801	4.751	0.185
DB5	1.131	0.573	1.210	0.984	2.895	0.132

TABLE V
COMPUTATIONAL COST (MILLISECOND) ON RASPBERRYPI 3B USING SVM

Stage	TD	TDs	mDWT	mDWTs	NMF	SPD
Preprocessing	0.296	0.293	0.285	0.294	0.289	0.293
Feature extraction	21.222	5.704	15.461	14.012	49.769	2.457
Training	1.911	1.962	1.256	1.950	2.032	0.753
Prediction	2.735	2.906	1.959	2.701	2.567	1.129
Online	24.253	8.903	17.705	17.007	52.625	3.879

TD and mDWT is evaluated using a laptop (CPU: Intel i7-10875H, 2.3GHz, eight-core 16 threads RAM: 32G). The computational time for feature extraction of every sample on average is calculated.

The result is illustrated in Table IV. It shows that the computational cost of the SPD manifold method is about 3.01%∼11.67%, 10.36%∼13.51%, and 2.90%∼4.52% of TD, mDWT, and NMF, respectively, which is less than 14% against contrast methods. For TDs and mDWTs, the ratio of time cost is 23.04%∼40.65%, 13.41%∼24.16% of the SPD manifold method, which reduces computational cost with a decrease in accuracy. Less computation cost can be observed for the proposed method against the contrast group.

The computational cost of every stage is also tested on Raspberry Pi 3B using *OYData* and SVM classifier, as shown in Table V. The online processing time is calculated by summarizing the time of preprocessing, feature extraction, and model prediction. The feature extraction time and the online prediction time on a Raspberry Pi 3B of the proposed method are 4.94%∼43.08% and 7.37%∼43.57% of the contrast group. The feature extraction time takes a significant part of the online prediction process (63.34%∼94.57%), which shows the importance of feature extraction in the whole process.

TABLE VI
COMPARISON WITH RECENT MYOELECTRIC PATTERN RECOGNITION RESEARCH

Research	Participants	Gesture	Channel number	Method	Accuracy
[36]	40	6	8	Machine learning with multi-window majority Voting	80.70%
[37]	10	10	8	Deep learning	77.78%
[38]	12	9	16	Machine learning with the clustering-feedback method	82.60%
[39]	21	17	8	Machine learning with the sequential floating feature selection method	84.50%
[40]	4	7	8	Machine learning	89.20%
This work	10	11	8	Machine learning with SPD- manifold based features	**84.85%**

V. DISCUSSION

This work proposes an innovative approach for myoelectric pattern recognition with SPD manifold for non-Euclidean spatial structural feature extraction. Traditional features like TD and mDWT can reach remarkable performance to extract temporal features [26], [33], [34], but performance drops when they are used for spatial features extraction, as shown by the performance of TDs and mDWTs in this work. New methods like an SPD manifold are worth exploring to extract spatial features more effectively.

Hand gestures are classified using four machine learning algorithms, including LDA, QDA, SVM, and KNN, among which SVM shows superiority over the other three methods. The best performance on *OYData* reaches an accuracy of 84.85% achieved by SVM, which is significantly better than the contrast group with an improvement of about 4%∼20% under a significant level of p <0.005. The best performance on eleven gestures of *Ninapro* DB2, DB4, and DB5 reaches classification accuracy of 81.93%±5.96%, 81.75%±7.28%, and 84.52%±3.63%, with an improvement of about 2%∼20%. A similar trend in the F1-score is observed. The performance shows good university of the proposed method with various EMG sensors of public databases. Statistical significance analysis between the SPD manifold-based method and contrast methods reaches $p < 0.005$ on all pairs of groups, which shows significant improvement of the proposed method. The performance comparison with other recent machine learning-based studies is shown in Table VI. It shows that the presented approach is competitive with most recent research.

For the classical feature extraction method, a way to improve the classification performance is by combining more statistical features as a feature vector to acquire more affluent information inside EMG signals. Besides this, deep learning has been for myoelectric pattern recognition, aiming to extract

more informative features automatically and recognize EMG patterns in an end-to-end approach [7], [41]. However, these two techniques will increase the algorithms' complexity and the hardware cost to extract high-quality features. In this work, the time consumption comparison shows that the time cost of the SPD manifold-based method is less than the contrast method, which reduces the computational cost significantly, and explores a new way for EMG feature extraction. The fewer computational cost of the proposed method profit from two aspects: the lower dimension of SPD matrices than EMG envelopes and the Log-Euclidean Metric with low complexity. It is appliable in a low-cost system with embedded processors.

This work shows that the SPD manifold has good potential to extract informative structural representations from EMG signals in a time-efficient manner. It proves that the non-Euclidean SPD manifold has good potential in topological structure excavating from EMG signals. However, limitation still exists. For one thing, the shortcoming of the tangent space-based method is that it is the first-order approximation of curved data, which loses geometric information unavoidably. A better approach can be mapping the SPD matrix onto the Reproducing Kernel Hilbert Space (RKHS) [42] and finding a suitable kernel to describe the information inside EMG signals, which provides more sophisticated geometric descriptions of the SPD manifold. For another, this work only focuses on improving the classification performance and decreasing the computational cost, leaving robustness against factors like inter-session/subject, electrode shift, etc., unconcerned. Spatial representation can be a potential choice to improve the stableness of EMG pattern recognition in that the relative relationship between different EMG channels may be invariable and robust against disturbances. Combining domain adaption approach or incremental learning method with SPD manifold can be an innovative path for more appliable myoelectric pattern recognition systems in the future.

VI. Conclusion and Future Works

This work proposes an innovative approach for myoelectric pattern recognition with an SPD manifold. The spatial information within different channels of EMG signals is used for hand gesture recognition. The presented approach is compared with two classical feature extraction methods on eleven gestures from ten subjects using four machine learning classifiers. The best performance reaches an accuracy of 84.85%±5.15% and an F1-score of 84.95%±5.09% with the SPD manifold-based method and SVM classifier, which outperforms the contrast group by 4.04%∼20.25% with a significance level of p <0.005. Furthermore, the computational cost is far less than the contrast group. The performance is also tested on a subset of three public databases, and a similar superiority of the proposed method is achieved. It proves that the SPD manifold-based method is effective and efficient, which provides a novel way for EMG pattern recognition.

In the future, more efforts need to be made to design better algorithms based on the SPD manifold. The SPD matrix will be projected to the high-dimensional RKHS to find more appropriate representations. Domain adaption techniques and incremental learning methods will be integrated into the scheme to improve the robustness and stability of the algorithm. The performance of high-density EMG signals will be analyzed. Furthermore, fusing with other modal information like computer vision with EMG signals and designing a unified decoding framework with SPD manifold can also be a good choice to develop more convenient human-machine interfaces.

References

[1] R. Merletti and P. A. Parker, *Electromyography: Physiology, Engineering, and Noninvasive Applications*. New York, NY, USA: Wiley, 2004.

[2] Y.-L. Chen, I.-J. Yang, L.-C. Fu, J.-S. Lai, H.-W. Liang, and L. Lu, "IMU-based estimation of lower limb motion trajectory with graph convolution network," *IEEE Sensors J.*, vol. 21, no. 21, pp. 24549–24557, Nov. 2021.

[3] G. Chen *et al.*, "A novel illumination-robust hand gesture recognition system with event-based neuromorphic vision sensor," *IEEE Trans. Autom. Sci. Eng.*, vol. 18, no. 2, pp. 508–520, Apr. 2021.

[4] E. Ayodele *et al.*, "Grasp classification with weft knit data glove using a convolutional neural network," *IEEE Sensors J.*, vol. 21, no. 9, pp. 10824–10833, May 2021.

[5] Q. Ding, X. Zhao, J. Han, C. Bu, and C. Wu, "Adaptive hybrid classifier for myoelectric pattern recognition against the interferences of outlier motion, muscle fatigue, and electrode doffing," *IEEE Trans. Neural Syst. Rehabil. Eng.*, vol. 27, no. 5, pp. 1071–1080, May 2019.

[6] K. O. Thielbar *et al.*, "Benefits of using a voice and EMG-driven actuated glove to support occupational therapy for stroke survivors," *IEEE Trans. Neural Syst. Rehabil. Eng.*, vol. 25, no. 3, pp. 297–305, Mar. 2017.

[7] W. Guo *et al.*, "Long exposure convolutional memory network for accurate estimation of finger kinematics from surface electromyographic signals," *J. Neural Eng.*, vol. 18, no. 2, Mar. 2021, Art. no. 026027.

[8] K. Li, J. Zhang, L. Wang, M. Zhang, J. Li, and S. Bao, "A review of the key technologies for sEMG-based human-robot interaction systems," *Biomed. Signal Process. Control*, vol. 62, Sep. 2020, Art. no. 102074.

[9] M. Jordanic, M. Rojas-Martínez, M. A. Mañanas, and J. F. Alonso, "Spatial distribution of HD-EMG improves identification of task and force in patients with incomplete spinal cord injury," *J. NeuroEng. Rehabil.*, vol. 13, no. 1, p. 11, Apr. 2016.

[10] H.-B. Xie, P. Zhou, T. Guo, B. Sivakumar, X. Zhang, and S. Dokos, "Multiscale two-directional two-dimensional principal component analysis and its application to high-dimensional biomedical signal classification," *IEEE Trans. Biomed. Eng.*, vol. 63, no. 7, pp. 1416–1425, Jul. 2016.

[11] M. Ison and P. Artemiadis, "The role of muscle synergies in myoelectric control: Trends and challenges for simultaneous multifunction control," *J. Neural Eng., Rev.*, vol. 11, no. 5, Oct. 2014, Art. no. 051001.

[12] D. Xiong, D. Zhang, X. Zhao, Y. Chu, and Y. Zhao, "Synergy-based neural interface for human gait tracking with deep learning," *IEEE Trans. Neural Syst. Rehabil. Eng.*, vol. 29, pp. 2271–2280, 2021.

[13] R. Zhuang, Z. Ma, W. Feng, and Y. Lin, "SPD data dictionary learning based on kernel learning and Riemannian metric," *IEEE Access*, vol. 8, pp. 61956–61972, 2020.

[14] O. Yair, M. Ben-Chen, and R. Talmon, "Parallel transport on the cone manifold of SPD matrices for domain adaptation," *IEEE Trans. Signal Process.*, vol. 67, no. 7, pp. 1797–1811, Apr. 2019.

[15] O. Tuzel, F. Porikli, and P. Meer, "Pedestrian detection via classification on Riemannian manifolds," *IEEE Trans. Pattern Anal. Mach. Intell.*, vol. 30, no. 10, pp. 1713–1727, Oct. 2008.

[16] Z. Gao, Y. Wu, M. Harandi, and Y. Jia, "A robust distance measure for similarity-based classification on the SPD manifold," *IEEE Trans. Neural Netw. Learn. Syst.*, vol. 31, no. 9, pp. 3230–3244, Sep. 2020.

[17] A. Das, M. S. Nair, and S. D. Peter, "Sparse representation over learned dictionaries on the Riemannian manifold for automated grading of nuclear pleomorphism in breast cancer," *IEEE Trans. Image Process.*, vol. 28, no. 3, pp. 1248–1260, Mar. 2019.

[18] F. Tang, M. Fan, and P. Tino, "Generalized learning Riemannian space quantization: A case study on Riemannian manifold of SPD matrices," *IEEE Trans. Neural Netw. Learn. Syst.*, vol. 32, no. 1, pp. 281–292, Jan. 2021.

[19] Z. Huang *et al.*, "Geometry-aware similarity learning on SPD manifolds for visual recognition," *IEEE Trans. Circuits Syst. Video Technol.*, vol. 28, no. 10, pp. 2513–2523, Oct. 2018.

[20] R. Wang, X.-J. Wu, and J. Kittler, "SymNet: A simple symmetric positive definite manifold deep learning method for image set classification," *IEEE Trans. Neural Netw. Learn. Syst.*, vol. 33, no. 5, pp. 2208–2222, May 2022, doi: 10.1109/TNNLS.2020.3044176.
[21] F. Nielsen and R. Bhatia, *Matrix Information Geometry*. Cham, Switzerland: Springer, 2013.
[22] A. Barachant, S. Bonnet, M. Congedo, and C. Jutten, "Multiclass brain–computer interface classification by Riemannian geometry," *IEEE Trans. Biomed. Eng.*, vol. 59, no. 4, pp. 920–928, Apr. 2012.
[23] V. Arsigny, P. Fillard, X. Pennec, and N. Ayache, "Geometric means in a novel vector space structure on symmetric positive-definite matrices," *SIAM J. Matrix Anal. Appl.*, vol. 29, no. 1, pp. 328–347, Jan. 2007.
[24] X. Pennec, P. Fillard, and N. Ayache, "A Riemannian framework for tensor computing," *Int. J. Comput. Vis.*, vol. 66, no. 1, pp. 41–66, Jan. 2006.
[25] A. Cherian, S. Sra, A. Banerjee, and N. Papanikolopoulos, "Jensen–Bregman LogDet divergence with application to efficient similarity search for covariance matrices," *IEEE Trans. Pattern Anal. Mach. Intell.*, vol. 35, no. 9, pp. 2161–2174, Sep. 2013.
[26] M. Atzori *et al.*, "Electromyography data for non-invasive naturally-controlled robotic hand prostheses," *Sci. Data*, vol. 1, no. 1, pp. 1–13, Dec. 2014.
[27] A. Gijsberts, M. Atzori, C. Castellini, H. Müller, and B. Caputo, "Movement error rate for evaluation of machine learning methods for sEMG-based hand movement classification," *IEEE Trans. Neural Syst. Rehabil. Eng.*, vol. 22, no. 4, pp. 735–744, Jan. 2014.
[28] S. Pizzolato, L. Tagliapietra, M. Cognolato, M. Reggiani, H. Müller, and M. Atzori, "Comparison of six electromyography acquisition setups on hand movement classification tasks," *PLoS ONE*, vol. 12, no. 10, pp. 1–7, 2017.
[29] O. Tuzel, F. Porikli, and P. Meer, "Pedestrian detection via classification on Riemannian manifolds," *IEEE Trans. Pattern Anal. Mach. Intell.*, vol. 30, no. 10, pp. 1713–1727, Oct. 2008.
[30] H. Hotelling, "Analysis of a complex of statistical variables into principal components," *Brit. J. Educ. Psychol.*, vol. 24, no. 6, pp. 417–520, 1933.
[31] S. Pancholi and A. M. Joshi, "Portable EMG data acquisition module for upper limb prosthesis application," *IEEE Sensors J.*, vol. 18, no. 8, pp. 3436–3443, Apr. 2018.
[32] F. Pedregosa *et al.*, "Scikit-learn: Machine learning in Python," *J. Mach. Learn. Res.*, vol. 12, pp. 2825–2830, Oct. 2011.
[33] A. Pradhan, J. He, and N. Jiang, "Performance optimization of surface electromyography based biometric sensing system for both verification and identification," *IEEE Sensors J.*, vol. 21, no. 19, pp. 21718–21729, Oct. 2021.
[34] F. Duan *et al.*, "sEMG-based identification of hand motion commands using wavelet neural network combined with discrete wavelet transform," *IEEE Trans. Ind. Electron.*, vol. 63, no. 3, pp. 1923–1934, Mar. 2016.
[35] U. Côé-Allard *et al.*, "Deep learning for electromyographic hand gesture signal classification using transfer learning," *IEEE Trans. Neural Syst. Rehabil. Eng.*, vol. 27, no. 4, pp. 760–771, Apr. 2019.
[36] M. F. Wahid, R. Tafreshi, and R. Langari, "A multi-window majority voting strategy to improve hand gesture recognition accuracies using electromyography signal," *IEEE Trans. Neural Syst. Rehabil. Eng.*, vol. 28, no. 2, pp. 427–436, Feb. 2020.
[37] X. Zhang, Z. Yang, T. Chen, D. Chen, and M.-C. Huang, "Cooperative sensing and wearable computing for sequential hand gesture recognition," *IEEE Sensors J.*, vol. 19, no. 14, pp. 5775–5783, Jul. 2019.
[38] Y. Fang, D. Zhou, K. Li, and H. Liu, "Interface prostheses with classifier-feedback-based user training," *IEEE Trans. Biomed. Eng.*, vol. 64, no. 11, pp. 2575–2583, Nov. 2017.
[39] F. S. Botros, A. Phinyomark, and E. J. Scheme, "Electromyography-based gesture recognition: Is it time to change focus from the forearm to the wrist?" *IEEE Trans. Ind. Informat.*, vol. 18, no. 1, pp. 174–184, Jan. 2022.
[40] S. Benatti *et al.*, "A versatile embedded platform for EMG acquisition and gesture recognition," *IEEE Trans. Biomed. Circuits Syst.*, vol. 9, no. 5, pp. 620–630, Oct. 2015.
[41] D. Xiong, D. Zhang, X. Zhao, and Y. Zhao, "Deep learning for EMG-based human-machine interaction: A review," *IEEE/CAA J. Autom. Sinica*, vol. 8, no. 3, pp. 512–533, Mar. 2021.
[42] R. Zhuang, Z. Ma, W. Feng, and Y. Lin, "SPD data dictionary learning based on kernel learning and Riemannian metric," *IEEE Access*, vol. 8, pp. 61956–61972, 2020.